

Shear Localization in a Model Glass

F. Varnik,¹ L. Bocquet,² J.-L. Barrat,² and L. Berthier³

¹CECAM, ENS-Lyon, 46 Allée d'Italie, 69007 Lyon, France

²Département de Physique des Matériaux, Université Lyon I and CNRS, 69622 Villeurbanne CEDEX, France

³Theoretical Physics, Oxford University, 1 Keble Road, Oxford, OX1 3NP, United Kingdom

(Received 13 August 2002; published 3 March 2003)

Using molecular dynamics simulations, we show that a simple model of a glassy material exhibits the shear localization phenomenon observed in many complex fluids. At low shear rates, the system separates into a fluidized shear band and an unsheared part. The two bands are characterized by a very different dynamics probed by a local intermediate scattering function. Furthermore, a stick-slip motion is observed at very small shear rates. Our results, which open the possibility of exploring complex rheological behavior using simulations, are compared to recent experiments on various soft glasses.

DOI: 10.1103/PhysRevLett.90.095702

PACS numbers: 64.70.Pf, 05.70.Ln, 83.60.Df, 83.60.Fg

Shear localization is a commonly observed phenomenon in the rheology of complex fluids. Over some range of shear rates, a fluid undergoing simple shear flow in, for example, a Couette cell tends to separate into bands parallel to the flow direction, with high shear rate regions coexisting with smaller shear rate regions. In some cases [1], this shear-banding phenomenon can be understood in terms of underlying structural changes in the fluid, analogous to a first order phase transition. In other systems, however, no such changes are evident, and coexistence appears between a completely steady region (zero shear rate) and a sheared, fluid region. This second type of behavior has been observed [2–6], in particular, in systems of the so-called “soft glass” type [7]. Such systems include dense colloidal pastes, granular materials, emulsions, etc., Their rheological behavior is essentially determined by the competition between an intrinsic slow dynamics and the acceleration caused by the external flow [7–9]. The large time scales inherent to the glassy state manifest themselves in the nonlinear character of the rheological properties as a function of the shear rate $\dot{\gamma}$: existence of a yield stress (the system does not flow until the stress σ exceeds a threshold value σ_y) and nonlinear flow curves $\sigma = \sigma(\dot{\gamma})$.

The observation of strong heterogeneities in the flow of such systems suggests that a global flow curve is not sufficient to fully characterize the flow behavior. Indeed, a simple shear-thinning behavior would in general imply homogeneous shear flow in a planar Couette cell, since the shear stress is constant across the cell. More generally, it remains to clarify if these observations in systems with very different microscopic interactions are intrinsic to glassy dynamics, that is, if a generic scenario for inhomogeneous shear flow can be proposed, as attempted in several recent studies [10,11].

In order to investigate this issue, we performed molecular dynamics simulations of a generic glass forming system, consisting of an 80:20 binary mixture of *A* and *B* particles interacting via a Lennard-Jones potential, $U_{LJ}(r) = 4\epsilon_{\alpha\beta}[(\sigma_{\alpha\beta}/r)^{12} - (\sigma_{\alpha\beta}/r)^6]$, with $\alpha, \beta = A, B$.

The parameters ϵ_{AA} , σ_{AA} , and m_A define the units of energy, length, and mass. The unit of time is then given by $\tau = \sigma_{AA}\sqrt{m_A/\epsilon_{AA}}$. Furthermore, we choose $\epsilon_{AB} = 1.5\epsilon_{AA}$, $\epsilon_{BB} = 0.5\epsilon_{AA}$, $\sigma_{AB} = 0.8\sigma_{AA}$, $\sigma_{BB} = 0.88\sigma_{AA}$, and $m_B = m_A$. All simulations have been carried out at a fixed density of $\rho = 1.2$. This model system has been extensively studied [8,9,12] and exhibits, in the bulk state, a computer glass transition (in the sense that the relaxation time becomes larger than typical simulation times) at a temperature $T_c \approx 0.435$ [12].

We first equilibrate a large simulation box with periodic boundary conditions in all directions, at $T = 0.5$. The system is then quenched to a temperature below T_c . Most of the results discussed in this Letter correspond to $T = 0.2$. At this temperature, the structural relaxation times are orders of magnitude larger than at T_c . On the time scale of computer simulations, the system is in a glassy state, in which its properties slowly evolve with time (aging). After a time of $t = 4 \times 10^4$ [2×10^6 molecular dynamics (MD) steps], we create two parallel solid boundaries by freezing all the particles outside two parallel *xy* planes at positions $z_{\text{wall}} = \pm L_z/2$ ($L_z = 40$). For each computer experiment, ten independent samples (each containing 4800 particles) are prepared using this procedure. Note that the system is homogeneous in the *xy* plane ($L_x = L_y = 10$). We thus compute the system properties as an average over particles within thin layers parallel to the wall.

An overall shear rate is imposed by moving in the *x* direction all the atoms of, for instance, the left wall ($z_{\text{wall}} = -20$) with a strictly constant velocity of U_{wall} . This defines the total shear rate $\dot{\gamma}_{\text{tot}} = U_{\text{wall}}/L_z$. Velocity profiles are recorded discarding transients (of typical duration $1/\dot{\gamma}$) associated with the start of the shear motion.

Our main observation is reported in Fig. 1. We find that, at low overall shear rates $\dot{\gamma}_{\text{tot}}$, the system separates into a homogeneously sheared band and a part which is essentially unsheared. Note that the velocity profiles are not symmetric with respect to the midplane. Rather, the shear band is localized close to one of the walls, so that a single

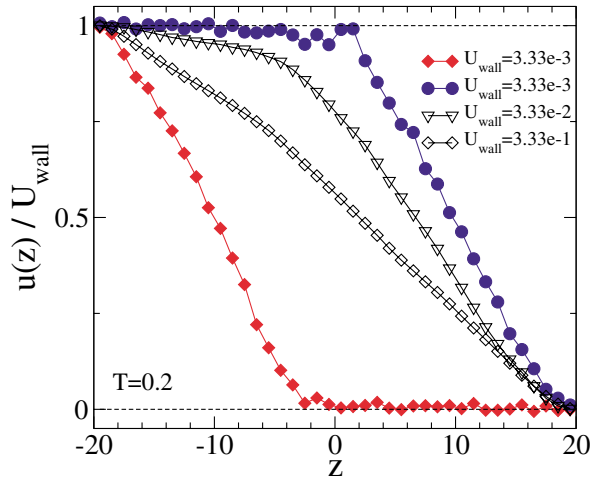


FIG. 1 (color online). Filled symbols: rescaled velocity profiles, $u(z)/U_{\text{wall}}$, from two independent simulation runs. In both cases, the left wall is moved with a constant velocity $U_{\text{wall}} = 3.33 \times 10^{-3}$ ($\dot{\gamma}_{\text{tot}} = 0.83 \times 10^{-4}$). Because of Galilean invariance, the sheared region may be located at either the moving or immobile wall. Open symbols: rescaled velocity profiles obtained at higher wall velocities $U_{\text{wall}} = 3.33 \times 10^{-2}$ and 3.33×10^{-1} corresponding to overall shear rates of $\dot{\gamma}_{\text{tot}} = 0.83 \times 10^{-3}$ and 0.83×10^{-2} . Note that the local shear rate of the sheared region is smaller at smaller U_{wall} .

interface between sheared and steady region is formed. The symmetry between the two walls, which is a result of Galilean invariance, is restored only on average, the shear band occurring equally likely on both sides of the simulation cell (see Fig. 1). A similar behavior has been observed in various experiments [2–6].

We observed oscillations of the velocity profile between the two mentioned solutions. This effect is possibly related to the finite size of the simulation box leading to a finite probability for the band to oscillate. In contrast, this probability would be zero for (very large) experimental systems, thus stabilizing one of the solutions. Within a given solution, we also observed fluctuations of the position of the interface between the two bands. These fluctuations increase with U_{wall} , so that at high U_{wall} the average velocity profile no longer exhibits a sharp separation between the jammed and the fluidized region (see

triangles in Fig. 1). A detailed discussion of these aspects is beyond the scope of this paper and we postpone it to a future report.

As shown in Fig. 1, the thickness h of the sheared region depends on the wall velocity U_{wall} . For very small U_{wall} , h is of the order of a few atomic diameters and varies only slightly with the wall velocity. As a consequence, the shear rate inside the sheared region, of order U_{wall}/h , increases with U_{wall} . As U_{wall} is further increased, h increases to reach the full slab size, $h = L_z$, at a given wall velocity, U_c . For $U_{\text{wall}} > U_c$, the velocity profile is therefore linear, as is observed in simple fluids. These findings are in qualitative agreement with experimental results on clay suspensions [3]. The rather slow variation of h with respect to a change of $\dot{\gamma}_{\text{tot}}$ at small wall velocities should, however, be contrasted to reports in [6]. However, the small size of our system compared to the width of interfacial regions makes a more quantitative analysis rather difficult for the moment. At a given global shear rate $\dot{\gamma}_{\text{tot}} = 10^{-4}$ ($U_{\text{wall}} = 0.004$), we also studied the influence of temperature on shear localization. We find that increasing the temperature is qualitatively similar to increasing the global shear rate: The thickness of the sheared region is an increasing function of the temperature. For example, $h \approx 20$ [see Fig. 1] at $T = 0.2$, whereas $h \approx 30$ at $T = 0.4$ and $h \approx L_z (= 40)$ at $T = 0.5$.

We find no obvious structural differences between the two regions of the sample. As shown in Fig. 2 (right panel), static properties such as the density profile, shear stress, and normal pressure are found to be constant across the film [13]. The distinction between the two bands is therefore purely dynamical. This can be seen for instance on the layer-resolved intermediate scattering function, $\phi_q(t; z) = \sum_i \langle \exp[iq_y [y_i(t) - y_i(0)]] \delta(z_i - z) \rangle$. We choose $q_y = 7.1$, which corresponds to the first maximum of the static structure factor. The left panel of Fig. 2 depicts $\phi_q(t; z)$ obtained from a simulation with $\dot{\gamma}_{\text{tot}} = 0.83 \times 10^{-4}$. One may first note the existence of two limiting behaviors of the correlation function, corresponding to the sheared and jammed regions, with a rather rapid change from one behavior to the other within a few layers. While in the jammed region (close to the right wall in Fig. 2) $\phi_q(t; z)$ barely relaxes, the

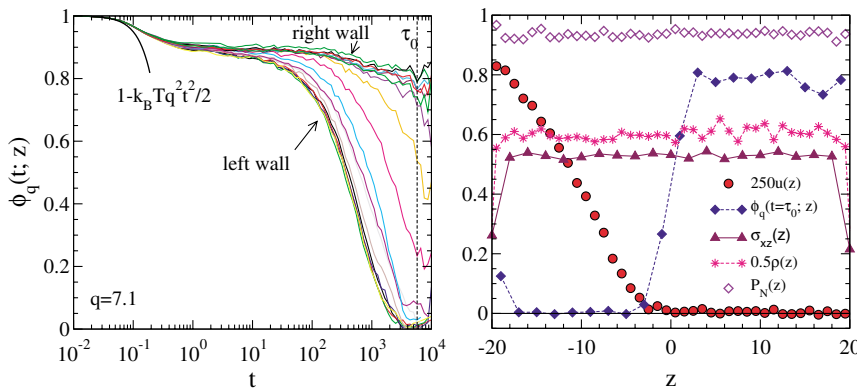


FIG. 2 (color online). Left panel: Intermediate scattering function, $\phi_q(t; z)$, computed within layers of thickness $dz = 2$. From bottom to top, $z = -17, -15, \dots, 15$. The temperature is $T = 0.2$, and $\dot{\gamma}_{\text{tot}} = 0.83 \times 10^{-4}$. The vertical dashed line marks the time $\tau_0 = 5754 \approx 0.5/\dot{\gamma}_{\text{tot}}$. Right panel: plot of $\phi_q(\tau_0; z)$ (connected diamonds), velocity profile (filled circles), local shear stress $\sigma_{xz}(z)$ (connected triangles), normal pressure $P_N(z)$ (open diamonds), and density profile $\rho(z)$ (connected stars).

correlation function in the sheared region (close to the left wall) exhibits a two-step relaxation as observed in homogeneously sheared systems. This observation reflects the acceleration of the structural relaxation due to the flow [9]. In the jammed region, the system behaves as a glassy solid, and $\phi_q(t; z)$ does not relax to zero on the simulation time scale.

A way to quantify the relation between the structural relaxation and the variation of the shear rate across the system is to look at the quantity $\phi_q(\tau_0; z)$, where τ_0 is of the order of $1/\dot{\gamma}_{\text{tot}}$. This quantity reflects the way the system has relaxed on the time scale imposed by the global shear rate. Results for $\phi_q(\tau_0; z)$ are shown in the right panel of Fig. 2. The change of the velocity profile, when going from the sheared towards the un-sheared region, is accompanied by a sharp jump in $\phi_q(\tau_0; z)$ at the interface between these two regions. The profile of $\phi_q(\tau_0; z)$ is very similar to that of an order parameter across an interface [14]. Other order parameters could be proposed to characterize the local dynamics: For example, the local relaxation time of $\phi_q(t; z)$, defined as the time after which $\phi_q(t; z)$ goes below a fraction of unity or the local diffusion coefficient parallel to the walls. All these definitions lead to a two-phase picture, with well-defined and spatially constant local characteristics in both phases.

In Fig. 3, we summarize the results by plotting the $\sigma(\dot{\gamma})$ flow curve of the model at $T = 0.2$. In this figure, we indicate the flow curve obtained for a system undergoing homogeneous shear flow, taken from Ref. [9]. We also show the points obtained for the same system driven by the boundaries, as described in the present paper. For a given global shear rate, $\dot{\gamma}_{\text{tot}}$, the shear stress corresponding to a localized solution is larger than the one in the homogeneous shear flow. This point can be understood by noting that, in the case of a boundary driven flow, the actual shear rate in the fluidized region is larger than $\dot{\gamma}_{\text{tot}}$

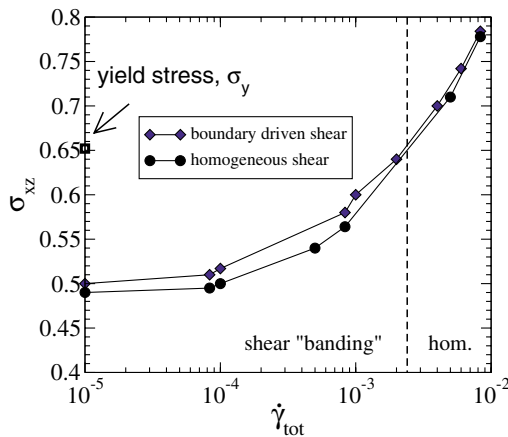


FIG. 3 (color online). Connected diamonds: σ_{xz} versus $\dot{\gamma}$ under homogeneous flow conditions at $T = 0.2$. Connected circles: σ_{xz} versus $\dot{\gamma}_{\text{tot}}$ in the boundary-driven shear flow. The vertical dashed line is an estimate of the global shear rate below which shear localization is expected.

and thus the corresponding shear stress slightly larger than that obtained by a homogeneous shear. We also note that no hysteresis is found in the flow curve as measured in our simulation: The same flow curve is obtained by increasing and decreasing the shear rate (not shown). It is interesting to note that, in the “banding regime,” the shear stress does not exhibit a plateau, in contrast to predictions of some recent phenomenological models [10,11]. This behavior can be traced back to the dependence of the local shear rate in the fluidized region as a function to $\dot{\gamma}_{\text{tot}}$.

To obtain the static yield stress, σ_y , we apply a small tangential force, F_T , acting on the left wall (treated as a rigid object with overdamped dynamics) for a certain amount of time, during which the velocity profile, $u(z)$, is sampled. The force on the wall is then slightly increased for a new measurement before going over to the next higher value. The static yield stress is then defined as the smallest force (per unit area) for which the average streaming velocity in the left half of the system, $u_{\text{av, left}} = \int_{-20}^0 u(z) dz / 20$, exceeds a minimum value, u_{min} . We empirically found that a measurement time of 4×10^3 [5×10^4 MD steps] and $u_{\text{min}} = 4.10^{-4}$ are reasonable choices in the sense that an increase of the measurement time or a decrease in u_{min} do not change σ_y significantly. Again, for each initial configuration, the system is first equilibrated at $T = 0.5$ before being quenched to a temperature below $T_c = 0.435$. The system is then propagated with $F_T = 0$ for a time t_w before the very first increment of the tangential force. At $T = 0.2$ and using an increment of $dF = 0.02$ (once in 5×10^4 MD steps), we have obtained $\sigma_y = 0.596 \pm 0.022$, 0.658 ± 0.009 , and 0.652 ± 0.015 corresponding to waiting times of $t_w = 10^3$, 4×10^3 , and 4×10^4 , respectively. Thus, already at a waiting time of $t_w = 4 \times 10^3$, aging effects on σ_y are negligible at the temperature studied. Note that, due to aging effects, σ_y might also depend on the speed at which the threshold value of the tangential force is reached. Therefore, we have determined σ_y for a higher value of $dF_T = 0.05$ in the case of $T = 0.2$ and $t_w = 4 \times 10^4$. This gives $\sigma_y = 0.66 \pm 0.015$ which agrees well with 0.652 ± 0.015 within the error bars.

It can be seen in Fig. 3 that $\sigma_y > \sigma(\dot{\gamma}_{\text{tot}} \rightarrow 0)$. Therefore, shear banding can be expected in the region limited by the vertical dotted line, which corresponds to $\sigma(\dot{\gamma}_{\text{tot}}) < \sigma_y$. Once the yield stress σ_y is added to the flow curve, the shear rate becomes multivalued in a range of shear stress, a situation encountered in several complex fluids [1]. This is the very origin of the shear banding we observe. As a consequence, this phenomenon should be generic for many soft glassy materials.

Finally, in the very low shear rate region, we observe a time dependence of the shear stress characteristic of stick-slip behavior, as demonstrated in Fig. 4. This is reminiscent to what is observed in friction simulations [15]. Because of numerical limitations, the limit between continuum sliding and stick-slip behavior could not be

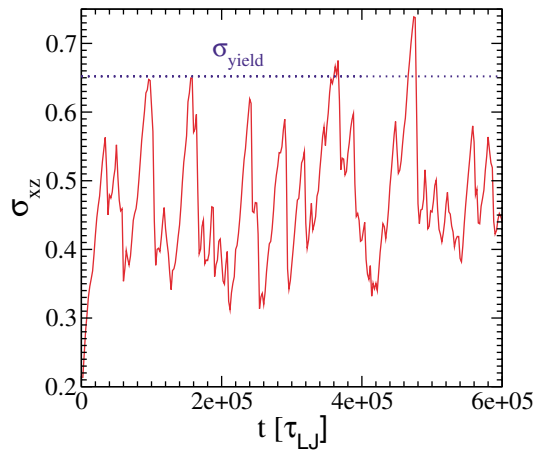


FIG. 4 (color online). Shear stress versus time for $\dot{\gamma}_{\text{tot}} = 0.83 \times 10^{-6}$ at $T = 0.2$. The stress rises up to a value close to $\sigma_y \approx 0.65$, before suddenly dropping to a value smaller than the one obtained in a homogeneous flow ($\sigma_{xz} \approx 0.4$).

precisely located. Qualitatively, this behavior is obtained when the thickness of the sheared layer h becomes of the order of a few particle diameters, which also corresponds to the width of the interface separating the sheared and jammed regions.

Our results lead to the following picture. (i) For global shear rates $\dot{\gamma}_{\text{tot}}$ smaller than a critical value, $\dot{\gamma}_c = U_c/L_z$, the system separates spatially into two regions, one with a finite, approximately uniform, shear rate, the other being jammed; (ii) when the total shear rate is increased, the thickness of the sheared region increases; (iii) for $\dot{\gamma}_{\text{tot}} > \dot{\gamma}_c$, h reaches the thickness of the slab, so that the flow is homogeneous with a linear velocity profile; (iv) at very small total shear rates, a stick-slip phenomenon is obtained; (v) the flow profile closely follows the local dynamics of the material, the strongly sheared region corresponding to a rapid structural relaxation, the jammed region to a glassy solid. The qualitative agreement of these phenomena with experimental observations in very different systems is remarkable: Ref. [3] describes explicitly the same scenario for the flow behavior of a clay suspension, including the stick-slip at very small shear rates. A more quantitative study of the flow profiles has been performed in Ref. [6] using a magnetic resonance imaging technique, confirming the existence of well-defined jammed and flow regions, whose relative width depends on the global shear rate. In contrast to molecular simulations, an experimental determination of velocity profiles together with a local probe of the dynamics is difficult, which makes the observation of such effects in simulations particularly promising. Our results also constrain phenomenological descriptions of the flow scenario. It is important to remark that models relating the local shear stress to the local shear rate, as $\sigma = \sigma_c + \alpha \dot{\gamma}^n$ (α being a constant and $n = 1$ corre-

sponding to Bingham fluids, and $n < 1$ to Herschel-Buckley fluids), are unable to account for these results. As emphasized above, the shear stress is constant throughout the Couette cell, so that any of the aforementioned models would predict a constant shear rate in the cell, in contrast to the present results. It appears therefore necessary to include explicitly nonlocal terms in phenomenological descriptions [1,10]. The existence of a close connection between velocity profile and local dynamics supports some of the assumptions of recent approaches treating the local “fluidity” of the system as an “order parameter” [11]. More detailed simulations, with systematic investigation of size effects, should allow a direct comparison with the predictions of such models.

F.V. is supported by the DFG (Grant No. VA 205/1-1) and by the CECAM. L.B. is supported by the EPSRC. Generous grants of computing time by the ZDV-Mainz and PSMN-Lyon are also acknowledged.

-
- [1] See, e.g., C.-Y. David Lu, P.D. Olmsted, and R.C. Ball, *Phys. Rev. Lett.* **84**, 642 (2000), which also contains many references to relevant experimental work.
 - [2] L.J. Chen, B.J. Ackerson, and C.F. Zukowski, *J. Rheol.* **38**, 193 (1993).
 - [3] F. Pignon, A. Magnin, and J.-M. Piau, *J. Rheol.* **40**, 573 (1996).
 - [4] W. Losert, L. Bocquet, T.C. Lubensky, and J.P. Gollub, *Phys. Rev. Lett.* **85**, 1428 (2000).
 - [5] G. Debrégeas, H. Tabuteau, and J.-M. di Meglio, *Phys. Rev. Lett.* **87**, 178305 (2001).
 - [6] P. Coussot *et al.*, *Phys. Rev. Lett.* **88**, 218301 (2002).
 - [7] P. Sollich, F. Lequeux, P. Hébraud, and M.E. Cates, *Phys. Rev. Lett.* **78**, 2020 (1997); S.M. Fielding, P. Sollich, and M.E. Cates, *J. Rheol.* **44**, 323 (2000).
 - [8] L. Berthier, J.-L. Barrat, and J. Kurchan, *Phys. Rev. E* **61**, 5464 (2000); J.-L. Barrat and L. Berthier, *Phys. Rev. E* **63**, 012503 (2000).
 - [9] L. Berthier and J.-L. Barrat, *J. Chem. Phys.* **116**, 6228 (2002); *Phys. Rev. Lett.* **89**, 095702 (2002).
 - [10] J.K.G. Dhont, *Phys. Rev. E* **60**, 4534 (1999); X.F. Yuan, *Europhys. Lett.* **46**, 542 (1999).
 - [11] G. Picard, A. Ajdari, L. Bocquet, and F. Lequeux, *Phys. Rev. E* **66**, 051501 (2002); cond-mat/0206260.
 - [12] W. Kob and H.C. Andersen, *Phys. Rev. E* **52**, 4134 (1995); W. Kob, *J. Phys. Condens. Matter* **11**, R85 (1999), and references therein. Our unit of time is $\sqrt{m\sigma^2/\epsilon}$, differing by a factor $\sqrt{48}$ from the one used in this reference.
 - [13] Local shear stress and normal pressure are computed using Irving-Kirkwood formulas; see, e.g., B.D. Todd, D.J. Evans, and P.J. Daivis, *Phys. Rev. E* **52**, 1627 (1995).
 - [14] S. Butler and P. Harrowell, *Nature (London)* **415**, 1008 (2002).
 - [15] M.O. Robbins and M.H. Müser, in *Modern Tribology Handbook*, edited by B. Bhushan (CRC Press, Boca Raton, FL, 2001).